# ADAPTIVE UNSTRUCTURED MESHING TECHNIQUE FOR BUILT-UP STRUCTURES

Pramote Dechaumphai*
Chulalongkorn University
Bangkok, Thailand

## Abstract

An adaptive unstructured meshing technique for thermal stress analysis of built-up structures has been developed. A finite element formulation for a triangular membrane element and a new plate bending element, used for modelling such structures under both mechanical and thermal loadings, is presented. The associated finite element matrices have been derived in closed form. The performance of the new plate bending element is evaluated for a plate with temperature gradient through its thickness by comparing the predicted solution with the exact solution. The effectiveness of the adaptive unstructured meshing technique combining with the finite element method is evaluated by two applications: (1) a stress analysis of a panel with a circular cutout, and (2) a thermal stress analysis of a built-up structure with intersecting panels. The adaptive mesh solutions for these two applications are compared with an exact solution and a fine mesh solution, respectively. These applications demonstrate that, without a priori knowledge of the solution, the adaptive unstructured meshing technique generates refined elements only in the regions needed to provide accurate solution at a reduced problem size and analysis computational time as compared to the results produced by the standard finite element procedure.

## Nomenclature

| | |
|---|---|
| A | finite element area |
| [B] | strain-displacement matrix |
| [C] | material stiffness matrix |
| E | modulus of elasticity |
| {F} | load vector |
| h | nodal spacing |
| [K] | stiffness matrix |
| M | bending moment |
| [N] | element interpolation function matrix |
| p | pressure |
| $\{S_1\}$, $\{S_2\}$ | vector of stress components |
| T | temperature |
| $T_o$ | reference temperature for zero stress |
| t | element thickness |
| u, v, w | displacement components |
| x, y, z | local coordinate directions |
| X, Y, Z | global coordinate directions |
| $\alpha$ | coefficient of thermal expansion |
| $\{\alpha\}$ | vector of coefficients of thermal expansion |
| $\{\delta\}$ | vector of element nodal unknowns |
| $\{\varepsilon\}$ | vector of strain components |
| $\lambda$ | eigenvalue |
| $\nu$ | Poisson's ratio |
| $\phi$ | key parameter for remeshing |
| $\sigma_x$, $\sigma_y$, $\tau_{xy}$ | stress components |
| $\sigma_1$, $\sigma_2$ | principal stress components |

### Subscripts

| | |
|---|---|
| b | bending |
| m | membrane |
| p | pressure |
| T | thermal |

### Superscripts

| | |
|---|---|
| T | transpose |

## Introduction

Accurate prediction of the structural response induced by both mechanical and thermal loadings is an important factor in the design of structures. Intense pressure and heat transfer rates may produce severe stresses that reduce the structural performance and may cause structural failure. Research is underway to improve the efficiency and accuracy of the thermal stress analysis procedure.

An adaptive unstructured meshing technique[1] has been shown to improve the efficiency and accuracy[2] of the high speed flow analysis, the thermal and structural analyses of continuum structures in two dimensions by the finite element method. The technique generates a new mesh based on the solution obtained from an earlier mesh. The new mesh consists of small elements in the regions with large changes in solution gradients and large elements in other regions where the gradient changes are small. Because the technique generates proper element sizes automatically, it is especially suitable for complex problems where a priori knowledge of the solutions does not exist.

Currently, the technique has been extended to construct adaptive meshes for structural analysis of "built-up" structures. Such structures are commonly modelled by using membrane and plate bending finite elements. A new triangular plate bending element to be used with the adaptive unstructured meshes for efficient thermal stress solution will be introduced in this paper. The paper, however, will concentrate on the evaluation of the adaptive unstructured meshing technique for providing solution accuracy as well as increasing computational efficiency for thermal stress analysis of structures.

*Associate Professor, Mechanical Engineering Department, Senior Member AIAA

The governing differential equations for predicting the structural response due to both thermal and mechanical loadings will be presented first. The triangular membrane element with temperature distribution over the element and a new triangular plate bending element with temperature gradient through the element thickness will be described. The corresponding finite element equations and the associated element matrices will be derived and presented. The basic concepts of the adaptive unstructured meshing technique and the selection of the meshing parameters used for construction of new meshes will be explained. Before applying the adaptive unstructured meshing technique to complex problems, the technique will be evaluated for the stress analysis of a panel with a circular cutout where the exact solution is available. The performance of the new triangular plate bending element under the thermal load will then be evaluated by an example of a plate with temperature gradient through its thickness in which the exact solution is also available. Finally the adaptive unstructured meshing technique for built-up structures will be evaluated by the thermal stress analysis of convectively-cooled intersecting panels in which the adaptive mesh solution will be compared with a fine mesh solution.

## Thermal Stress Analysis Procedure

### Governing Equations

The equations for the in-plane deformation and the transverse deflection of a plate that lies in a local x-y coordinate system are briefly described herein.

**In-Plane Deformation.** The equations for the in-plane deformation are given by the two-dimensional equilibrium equations in the form,

$$\frac{\partial}{\partial x}\{S_1\} + \frac{\partial}{\partial y}\{S_2\} = 0 \qquad (1)$$

where the vectors $\{S_1\}$ and $\{S_2\}$ consist of the stress components given by,

$$\{S_1\}^T = [\,\sigma_x \quad \tau_{xy}\,] \qquad \{S_2\}^T = [\,\tau_{xy} \quad \sigma_y\,] \qquad (2)$$

The stress components are related to the strain components and the temperature by the generalized Hooke's law,

$$\{\sigma\} = [C_m]\{\varepsilon\} - [C_m]\{\alpha\}(T(x,y) - T_o) \qquad (3)$$

where $\{\sigma\}$ contains the stress components $\sigma_x$, $\sigma_y$, and $\tau_{xy}$, $[C_m]$ is the material stiffness matrix, and $\{\alpha\}$ is the vector of the coefficients of thermal expansion. For the plane stress case, these material matrices are given in Ref. 3. The vector of the strain components is related to the displacement gradients given by,

$$\{\varepsilon\}^T = [\frac{\partial u}{\partial x} \quad \frac{\partial v}{\partial y} \quad \frac{\partial u}{\partial y} + \frac{\partial v}{\partial x}] \qquad (4)$$

**Transverse Deflection.** The equation for the transverse deflection in the z-direction normal to the x-y plane of the plate is given by the equilibrium equation[4] in the form

$$D\left(\frac{\partial^4 w}{\partial x^4} + 2\frac{\partial^4 w}{\partial x^2 \partial y^2} + \frac{\partial^4 w}{\partial y^4}\right) = -\frac{1}{1-\nu}\left(\frac{\partial^2 M_T}{\partial x^2} + \frac{\partial^2 M_T}{\partial y^2}\right) + p(x,y) \qquad (5)$$

where $D = Et^3/12(1-\nu^2)$ is the bending rigidity and $M_T$ is the thermal moment defined by

$$M_T = E\alpha\int_{-t/2}^{t/2}(T(z) - T_o)\,z\,dz \qquad (6)$$

### Derivation of Finite Element Equations

The Constant Strain Triangle (CST) and the Discrete Kirchoff Triangle (DKT) finite elements are used for the in-plane deformation and the transverse deflection, respectively.

**Constant Strain Triangle (CST).** The three-node CST element assumes a linear displacement distribution[3] over the element. The element equations can be derived by applying the method of weighted residuals to the governing differential equation, Eq. (1), which leads to the element equations in the form,

$$[K_m]\{\delta_m\} = \{F\} + \{F_m\} \qquad (7)$$

where the vector $\{\delta_m\}$ contains the element nodal unknowns of the in-plane displacements in the element local x-y coordinate directions. There are two in-plane displacements per node or six in-plane displacements per element. The element stiffness matrix, $[K_m]$, that appears in Eq. (7) is defined by,

$$[K_m] = [B_m]^T[C_m][B_m]\,t\,A \qquad (8)$$

where the strain-displacement interpolation matrix, $[B_m]$, can be derived easily and is given in Ref. 3. The first vector, $\{F\}$, on the right-hand-side of Eq. (7) contains the applied mechanical forces at element nodes. The second vector, $\{F_m\}$, consists of the equivalent nodal forces due to the thermal load. This second vector is defined by,

$$\{F_m\} = [B_m]^T[C_m]\{\alpha\}(T_{avg} - T_o)\,t\,A \qquad (9)$$

where $T_{avg}$ is the average element temperature.

**Discrete Kirchoff Triangle (DKT).** The three-node DKT element assumes a cubic distribution of the transverse deflection[5] over the element. The element equations can be derived by applying the method of weighted residuals to the plate bending equations, Eq. (5), which leads to the element equations in the form,

$$[K_b]\{\delta_b\} = \{F_p\} + \{F_b\} \qquad (10)$$

where the vector $\{\delta_b\}$ contains the element nodal unknowns of the transverse deflections and the rotations (slopes). Each node has a transverse deflection in the element local z-coordinate direction and two rotations about the element local x-y coordinate directions. Thus there are nine degrees of freedom per an element. The performance of the element has been evaluated thoroughly in Ref. 6 using several benchmark problems for bending of plates under the mechanical load. However, the performance of the element under the thermal load has not been evaluated. Without the thermal load, only the element stiffness matrix, $[K_b]$, and the nodal force vector due to the applied pressure, $\{F_p\}$, that appear in the element equations, Eq. (10), are needed. These matrices are defined by,

$$[K_b] = \int_A [B_b]^T [C_b] [B_b] \, dA \qquad (11)$$

$$\{F_p\} = \int_A [N_b]^T p \, dA \qquad (12)$$

where the strain-displacement interpolation matrix, $[B_b]$, the plate material stiffness matrix, $[C_b]$, and the plate element interpolation function matrix, $[N_b]$, are given in Refs. 5-6. The above two element matrices, $[K_b]$ and $\{F_p\}$, can be evaluated in closed form (i.e. numerical integration is not required) and the details of the derivation are given Refs. 6-7.

With the presence of the thermal load, the vector of the equivalent nodal forces due to the temperature change, $\{F_b\}$, is included in the element equations, Eq. (10). This additional vector is defined by,

$$\{F_b\} = \int_A [B_b]^T \{M\} \, dA \qquad (13)$$

where

$$\{M\}^T = [M_T \quad M_T \quad 0] \qquad (14)$$

In the above Eq. (14), the thermal moment $M_T$ is defined in Eq. (6). The vector of the equivalent nodal forces due to the thermal load, $\{F_b\}$, above can also be derived in closed form. For an element with arbitrary temperature distribution through the plate thickness, $T = T(z)$, this vector, $\{F_b\}$, is

$$\{F_b\} = M_T [G]^T \begin{Bmatrix} 1 \\ 1 \\ 0 \end{Bmatrix} \qquad (15)$$

where the matrix [G] has been derived and given in the Appendix.

Note that, for general built-up structures, elements can be arbitrarily oriented in three dimensions. Transformation of these element matrices from a local x-y-z coordinate system to a global X-Y-Z coordinate system is required prior assembling them to obtain a set of simultaneous equations. In such the global X-Y-Z coordinate system, each node has six degrees of freedom which are the three translations and the three rotations. The matrix transformation procedure, however, can be easily worked out and is not presented herein for brevity.

## Adaptive Unstructured Remeshing Procedure

### Remeshing Strategy

The basic idea of adaptive unstructured remeshing[1] is to construct a completely new mesh based on the solution obtained from the previous mesh. The new mesh will have small elements (short nodal spacings) in regions of large changes in solution gradients and large elements (large nodal spacings) in regions where the gradient changes are small. Proper nodal spacings used for constructing a new mesh are determined by following the solid mechanics concept of finding the principal stresses, $\sigma_1$ and $\sigma_2$, from a given state of stresses, $\sigma_x$, $\sigma_y$, and $\tau_{xy}$, i.e.,

$$\begin{bmatrix} \sigma_x & \tau_{xy} \\ \tau_{xy} & \sigma_y \end{bmatrix} \Rightarrow \begin{bmatrix} \sigma_1 & 0 \\ 0 & \sigma_2 \end{bmatrix} \qquad (16)$$

To construct an adaptive mesh for a structural problem, short nodal spacings are needed in the regions of large change in the stress gradients such as in stress concentration regions. Large nodal spacings can be used in other regions such as in the regions with fairly uniform stress. The stress is thus considered as a key parameter, denoted by $\phi$, for remeshing. At a typical node in the previous mesh, the second derivatives of the key parameter, $\phi$, (analogous to the stress components in Eq. (16)) are computed and the two eigenvalues (analogous to the principal stresses) are then determined,

$$\begin{bmatrix} \frac{\partial^2\phi}{\partial x^2} & \frac{\partial^2\phi}{\partial x \, \partial y} \\ \frac{\partial^2\phi}{\partial x \, \partial y} & \frac{\partial^2\phi}{\partial y^2} \end{bmatrix} \Rightarrow \begin{bmatrix} \lambda_1 & 0 \\ 0 & \lambda_2 \end{bmatrix} \qquad (17)$$

The larger eigenvalue, $\lambda = \max(\lambda_1, \lambda_2)$, is then selected for that node and the same process is repeated for all the other nodes in the previous mesh. Proper nodal spacings, denoted by h, used for constructing a new mesh are then determined from the condition required to produce an optimal mesh[1],

$$\lambda h^2 = \text{constant} = \lambda_{max} h_{min}^2 \qquad (18)$$

where $\lambda_{max}$ is the largest eigenvalue of all the nodes in the previous mesh and $h_{min}$ is the specified minimum nodal spacing for the new mesh.

The second derivatives of the key parameter, $\phi$, for remeshing appeared in Eq. (17) are determined using the following procedure. The first derivative (e.g. with respect to x) is assumed to vary over an element in the form,

$$\frac{\partial\phi}{\partial x} = [N] \left\{ \frac{\partial\phi}{\partial x} \right\} \qquad (19)$$

where the vector on the right-hand-side of the above equation contains the unknown nodal values of the first

derivatives. These unknown nodal values are obtained by solving,

$$\int_A \{N\}[N]\,dA \left\{\frac{\partial\phi}{\partial x}\right\} = \int_A \{N\}\,dA \frac{\hat{\partial\phi}}{\partial x} \qquad (20)$$

where $\hat{\partial\phi/\partial x}$ is the computed constant element gradient. The process is repeated to determine the second derivative $\partial^2\phi/\partial x^2$. Determination of the other second derivatives which appear in Eq. (17) is performed in the same fashion.

### Remeshing Parameters

The adaptive remeshing technique described requires a selection of proper key parameters ($\phi$ in Eq. (17)) for remeshing. For structural problems under the mechanical load alone, stress is an appropriate choice for the key parameter so that regions with high stress concentrations will be captured. However, the key parameter representing the stress should be a scalar quantity (directionally independent) such as the Von Mises stress defined in two dimensions by,

$$\sigma_{\text{Von Mises}} = \frac{1}{\sqrt{2}}\sqrt{(\sigma_x - \sigma_y)^2 + \sigma_x^2 + \sigma_y^2 + 6\tau_{xy}^2} \qquad (21)$$

For structural problems under both the mechanical and thermal loads, the structure temperature and the Von Mises stress should be used as the key parameters for remeshing simultaneously so that the mesh generated can accurately represent the prescribed temperature distribution and capture the high thermal stress as well as the mechanical stress concentration.

## Applications

Two applications are presented to demonstrate the effectiveness of the adaptive unstructured meshing technique and an example problem is presented to evaluate the performance of the DKT plate bending element under the thermal load. The capability of the adaptive unstructured meshing technique for providing accurate analysis solution is demonstrated in the first application for a panel with a circular cutout subjected to an in-plane force. The capability of the technique for reducing the problem size and the analysis computational time is demonstrated in the last application for the thermal stress analysis of a convectively cooled intersecting panel structure under severe temperature gradients.

### Panel With Circular Cutout

A panel with a circular cutout, shown in Fig. 1, is an ideal structure to demonstrate the capability of the adaptive unstructured meshing technique because closed-form solutions[8] are available. The panel is subjected to an applied uniform stress ($\sigma_o$) of 10 ksi in the longitudinal y-direction (see figure). The exact normal stress ($\sigma_y$) distribution along the x-direction at y=0 is given by,

$$\sigma_y = \frac{\sigma_o}{2}\left(2 + \frac{a^2}{x^2} + 3\frac{a^4}{x^4}\right) \qquad (22)$$

where a is the radius of the circular cutout. The peak stress ($3\sigma_o$) of 30 ksi occurs at the edge of the cutout (point A in the figure).

Due to symmetry, a quarter of the panel can be used in the analysis. An initial mesh was constructed which consists of 184 nodes and 306 triangles as shown in Fig. 2(a). Detail of the mesh near the cutout is shown in Fig. 2(b). With this mesh, the structural analysis (plane stress analysis with CST elements) was performed to predict the panel deformation and the stress distributions. The contours of the normal stress ($\sigma_y$) distribution in the longitudinal y-direction near the cutout are shown in Fig. 2(c). The peak predicted stress ($\sigma_y$) at the edge of the cutout obtained from this initial mesh is 19.5 ksi compared to the exact peak stress of 30 ksi. The 35% error in the peak stress is due to the coarse elements used near the cutout region.

The stress distribution in form of the Von Mises stress, Eq. (21), obtained from the initial mesh is used as the key parameter for remeshing to construct a new adaptive mesh. The new adaptive mesh, shown in Fig. 3(a), has fewer nodes and elements (149 nodes and 250 triangles) than the initial mesh (approximately 20% reduction in the number of unknowns). However, finer elements are concentrated in the region of high stress gradients near the cutout (shown in Fig. 3(b)) to provide a more accurate stress solution. The structural analysis is then performed and the contours of the normal stress ($\sigma_y$) distribution near the cutout are shown in Fig. 3(c). The peak predicted stress ($\sigma_y$) at the edge of the cutout is now 28.5 ksi which only 5% lower than the exact level of 30 ksi.

The normal stress ($\sigma_y$) distributions along the x-direction at y=0 obtained from the initial and the adaptive meshes are compared with the exact stress distribution as shown in Fig. 4. By defining a percentage error based on the $L_2$ norm in the form,

$$\%\ \text{error} = \frac{\left(\int_a^b [(\sigma_y)_{\text{Exact}} - (\sigma_y)_{\text{F.E.}}]^2\,dx\right)^{1/2}}{\left(\int_a^b [(\sigma_y)_{\text{Exact}}]^2\,dx\right)^{1/2}} \times 100 \qquad (23)$$

the figure shows that the solution error was reduced from 17% to 2% with one adaptive mesh. In addition, as the solution accuracy increased, the number of unknowns decreased, because finer elements are concentrated in the region of high stress gradients near the cutout where as large elements are used in other regions.

It is important to note that the adaptive meshing technique automatically generates refined elements in the regions of high stresses. A priori knowledge of the solution to the problem (e.g. high stress regions that require refined elements) is not needed before performing the analysis. The technique thus provides an advantage over the standard finite element procedure especially for more complex problems or larger structures (such as the structure which will be presented in the last example) where a priori knowledge of the solution does not exist.

## Plate Bending Due To Thermal Load

A free aluminum plate with temperature gradient through its thickness, shown in Fig. 5, is a simple example that can be used to measure the performance of the DKT plate bending element. The exact solution[4] for the transverse deflection is given by,

$$w(x,y) = -\frac{3 M_T}{4 E t^3}(x^2 + y^2) \qquad (24)$$

where $M_T$ is the thermal moment defined in Eq. (6). For a linear temperature distribution through the plate thickness with the temperature $T_T$ on the top surface and $T_B$ on the bottom surface, the thermal moment is given by,

$$M_T = \frac{E \alpha t^2}{12 (1 - \nu)}(T_T - T_B) \qquad (25)$$

Due to symmetry, a quarter of the plate can be used in the analysis. The finite element model consists of 32 DKT plate bending elements and 25 nodes with 5 nodes equally spaced in each x and y direction (shown in Fig. 5) is used to predict the plate bending response. By assuming the top and bottom surface temperatures of 630°R and 530°R, respectively, both the predicted finite element and the exact transverse deflection solutions along the x-direction at y=0 are compared in Fig. 6. The figure shows that the DKT plate bending elements provide exact transverse deflection solution to the problem.

It should be noted that, as described earlier in the finite element formulation section, all the DKT plate bending element matrices can be evaluated in closed form (i.e. numerical integration is not required). This simplifies the programming task, reduces the computational effort and eliminates numerical error that may occur in generating such element matrices. In addition, reference 6 has demonstrated the effectiveness of this element for providing solution accuracy for plate bending problems under different types of the mechanical load. The example presented herein endorses the performance of the DKT element and demonstrates its capability under the thermal load. The next example will combine the CST elements (used in the first example) and the DKT elements (used in this example) with the adaptive unstructured meshing technique for thermal stress analysis of a more complex built-up structure.

## Thermal Stress in Intersecting Panels

To demonstrate the capability of the adaptive unstructured meshing technique for thermal stress analysis of more complex structures, a three-dimensional structure which represents a scramjet engine inlet is considered. The structure experiences high heating from the impingement of an oblique shock from the vehicle forebody as illustrated in Fig. 7. The localized heatings result in high temperature gradients and their attendant thermal stresses in the engine panel. A typical "built-up" engine inlet structure, shown in the lower right corner of the figure, may consist of panels and stiffeners and may be actively cooled. To perform the thermal stress analysis of such structure, a finite element model consisting of plate bending and membrane elements for the panels and the stiffeners is required. Note that, in constructing such a finite element model, the same nodal discretization is also required along the interface between the stiffeners and the panels. Such task, combining with the requirement of placing refined elements at the high thermal stress regions for accurate thermal stress solution, is tedious. Furthermore, several modelling iterations may be needed before achieving the desired finite element model for solution accuracy.

For the purpose of demonstrating that accurate thermal stress solution can be obtained by using the adaptive unstructured meshing technique, both the structure temperature and the structural boundary conditions are prescribed as shown in Fig. 8. The prescribed temperature distribution simulates the structural temperature response from the high localized heating due to the shock impingement illustrated in Fig. 7. The peak temperature of 700 °R is assumed at the two "hot spot" regions with temperature distributions that exhibit high temperature gradients on both the panels and the stiffeners. Away from these two hot spot regions, the structure temperature is closed to the coolant temperature of 50 °R used for cooling the structure.

For most of the thermal stress problems, high compressive stresses normally occur at the high temperature and temperature gradient regions. Refined finite elements are thus needed in these regions. For more complex structures, high thermal stresses may also occur in other regions that have lower temperature or temperature gradients depending on the complexity of the structures and how they are constrained. Thus, in the standard finite element analysis procedure, a relatively fine finite element model is normally employed first to identify such high thermal stress regions. Because the thermal stress solution for this problem is not known and because a reference solution is needed for comparing with the adaptive mesh solutions (which will be presented later), a greatly fine finite element model was constructed as shown in Fig. 9(a). The model consists of 3,168 nodes (19,008 degrees of freedom) and 6,114 triangular elements.

The predicted thermal stress distribution in the Y-direction superimposed on the deformed geometry (greatly exaggerated), obtained from this fine finite element model, is shown in Fig. 9(b). As expected, high compressive stress with a magnitude of 25 ksi is at the two hot spot regions. However, a quite higher tensile stress with a magnitude of 54 ksi occurs between these two hot spot regions. Such phenomenon may not be anticipated prior analyzing the problem or before constructing the finite element model. This example demonstrates a need for an automated analysis procedure that can provide accurate solution without a priori knowledge of the solution to the problem.

The solution for this refine finite element model requires quite a large computational time (approximately 13 CPU hours on the VAX-8550 computer). This computational time can be reduced significantly by placing larger element sizes in the regions away from the hot spot regions. As mentioned earlier, construction of a finite element model with different element sizes while maintaining the same nodal discretization along the interface between various structural components is difficult. Furthermore, it is also difficult to construct a finite element model using all the four-node quadrilateral elements to satisfy such requirements and to achieve smooth transition of element sizes from the refined to the

coarse mesh regions. These difficulties can be alleviated and the analysis computational time can be reduced by the use of the adaptive unstructured meshing technique as will be described next.

Application of the adaptive unstructured meshing technique starts from constructing a fairly uniform mesh as shown in Fig. 10. This initial mesh consists of 547 nodes (3,282 degrees of freedom) and 994 triangular elements. With this mesh and the prescribed temperature distribution as shown in Fig. 8, the structural analysis was performed to predict the structure deformation and the stress distributions. The predicted thermal stress distribution in the Y-direction superimposed on the deformed geometry is shown in Fig. 11. The peak predicted compressive stress at the two hot spot is 20 ksi while the peak predicted tensile stress between the two hot spots is 33 ksi (approximately 40% lower than the fine mesh solution shown in Fig. 9). The computational time required by this initial mesh is about 15 minutes on the same VAX-8550 computer.

The temperature and the stress distribution (in form of the Von Mises stress given by Eq. (21)) obtained from the initial mesh are used as the meshing parameters to construct a new adaptive mesh. The new adaptive mesh, shown in Fig. 12, has slightly fewer nodes and elements (528 nodes and 989 elements) than the initial mesh. However, finer elements are concentrated in the high stress regions on both the panels and the stiffeners to provide solution accuracy. Coarser elements are generated in other regions to reduce the problem size and thus the computational time. The predicted thermal stress distribution in the Y-direction superimposed on the deformed geometry is shown in Fig. 13. The figure shows that the adaptive mesh model can provide the same stress solution accuracy as those obtained from the fine mesh model shown in Fig. 9 (i.e. the peak predicted tensile stress of 54 ksi is between the two hot spots that have compressive stresses of 25 ksi). However, the computational time required by the adaptive mesh model is only 15 minutes on the same VAX-8550 computer, a factor of 50 CPU time saving compared to that required by the fine mesh model.

The adaptive mesh model shown in Fig. 12 also highlights the ease of constructing a finite element model by using triangles. These triangles provide smooth transition of the element sizes from refined to coarse mesh regions. The smooth element transition enhances the thermal stress prediction with a more realistic distribution. This can be seen from the close resembling of the stress solution contours obtained from the adaptive mesh model (Fig. 13) and the fine mesh model (Fig. 9). This last application demonstrates the capability of the adaptive unstructured meshing technique that can provide accurate thermal stress solution at a reduced analysis computational cost without the knowledge of the solution prior performing the analysis.

## Concluding Remarks

An adaptive unstructured remeshing technique for thermal stress analysis of built-up structures has been developed. The technique generates a new mesh based on the solution obtained from a previous mesh. The new mesh consists of small elements in regions of large change in the stress gradients and large elements in other regions where the gradient changes are small. The finite element thermal stress formulation for the triangular membrane (CST) and plate bending (DKT) elements under both mechanical and thermal loadings is presented. All the element matrices were derived in closed form to simplify the programming task, reduce the computational time and eliminate error associated with the numerical integration. The adaptive unstructured meshing strategy was described and the procedure for determining nodal spacings needed for constructing a new adaptive mesh was explained. For thermal stress problems, both the temperature and the Von Mises stress are used simultaneously as the meshing parameters so that the new mesh generated can capture the high thermal stress as well as the mechanical stress concentration.

Two applications were presented to demonstrate the effectiveness of the adaptive unstructured meshing technique and an example problem was presented to evaluate the performance of the DKT plate bending element under the thermal load. The latter example problem demonstrates the capability of the DKT plate bending element that can provide exact transverse deflection solution for a free plate with linear temperature through its thickness. The two applications of a panel with a circular cutout (using CST elements) and a built-up structure with intersecting panels (using both CST and DKT elements) demonstrate the capability of the adaptive unstructured meshing technique that can: (1) help analysts to perform the analysis and achieve accurate solution without a priori knowledge of the solution; (2) alleviate the tedious, time-consuming task for analysts to construct suitable finite element models for complex built-up structures; (3) minimize the problem size by generating small elements in the regions with high solution gradients and large elements in the other regions automatically; and (4) provide smooth transition from refined to coarse mesh regions with the use of triangular elements that will further improve the stress prediction with a more realistic distribution.

The result from the examples presented in this paper have demonstrated the viability of the adaptive unstructured meshing technique combining with the finite element method to reduce the analysis manpower and computational effort as well as to provide accurate solutions to complex structural behavior.

## Appendix

The vector of the equivalent nodal forces due to the thermal load, $\{F_b\}$, for the DKT plate bending element given in Eq. (15) can be evaluated in closed form. This vector includes the matrix [G] given by,

$$[G] = \frac{1}{6}\begin{bmatrix} y_{31}[G_{11}] + y_{12}[G_{12}] \\ -x_{31}[G_{21}] - x_{12}[G_{22}] \\ -x_{31}[G_{11}] - x_{12}[G_{12}] + y_{31}[G_{21}] + y_{12}[G_{22}] \end{bmatrix}$$

The coefficients $x_{ij}$ and $y_{ij}$, i, j=1, 2, 3, are defined in terms of the element nodal coordinates by,

$$x_{ij} = x_i - x_j ; \qquad y_{ij} = y_i - y_j$$

The row matrices, $[G_{ij}]$, i,j=1,2, appeared in the matrix [G] above are given by,

$$[G_{11}] = \begin{bmatrix} p_5 & -q_5 & -r_5 \\ p_4 & q_4 & r_4 \\ -p_4-p_5 & q_4-q_5 & r_4-r_5 \end{bmatrix}$$

$$[G_{12}] = \begin{bmatrix} -p_6 & -q_6 & -r_6 \\ p_4+p_6 & q_4-q_6 & r_4-r_6 \\ -p_4 & q_4 & r_4 \end{bmatrix}$$

$$[G_{21}] = \begin{bmatrix} t_5 & 3-r_5 & q_5 \\ t_4 & -3+r_4 & -q_4 \\ -t_4-t_5 & r_4-r_5 & -q_4+q_5 \end{bmatrix}$$

$$[G_{22}] = \begin{bmatrix} -t_6 & 3-r_6 & q_6 \\ t_4+t_6 & r_4-r_6 & -q_4+q_6 \\ -t_4 & -3+r_4 & -q_4 \end{bmatrix}$$

The coefficients $p_k$, $q_k$, $r_k$ and $t_k$ are defined in Ref. 6.


## Acknowledgements

This work was performed when the author was employed at the Aerothermal Loads Branch, NASA Langley Research Center, Hampton, Virginia, U.S.A. The author wishes to thank his branch head, Dr. Allan R. Wieting, for his advice, support and encouragement.


## References


1. Peraire, J., Vahdati, M., Morgan, K. and Zienkiewicz, O. C., "Adaptive Remeshing for Compressible Flow Computations," Journal of Computational Physics, Vol. 72, 1987, pp. 449-466.

2. Dechaumphai, P., "Evaluation of an Adaptive Unstructured Remeshing Technique for Integrated Fluid-Thermal-Structural Analysis," Journal of Thermophysics and Heat Transfer, Vol. 5, No. 4, 1991, pp. 599-606.

3. Huebner, K. H. and Thornton, E. A., The Finite Element Method for Engineers, John Wiley & Sons, Inc. New York, 1982.

4. Boley, B. A. and Weiner, J. H., Theory of Thermal Stresses, John Wiley & Sons, Inc. New York, 1960.

5. Stricklin, J. A., Haisler, W. E., Tisdale, P. R. and Gunderson, R., "A Rapidly Converging Triangular Plate Element," AIAA Journal, Vol. 7, No. 1, 1969, pp. 180-181.

6. Batoz, J. L., Bathe, K. J. and Ho, L. W., "A Study of Three-Node Triangular Plate Bending Elements," International Journal for Numerical Methods in Engineering, Vol. 15, 1980, pp. 1771-1812.

7. Jeyachandrabose, C. and Kirkhope, J., "An Alternative Explicit Formulation for the DKT Plate-Bending Element," International Journal for Numerical Methods in Engineering, Vol. 21, 1985, pp. 1289-1293.

8. Timoshenko, S. P. and Goodier, J. N., Theory of Elasticity, Third Edition, McGraw-Hill Book Co., New York, 1934, pp. 90-97.


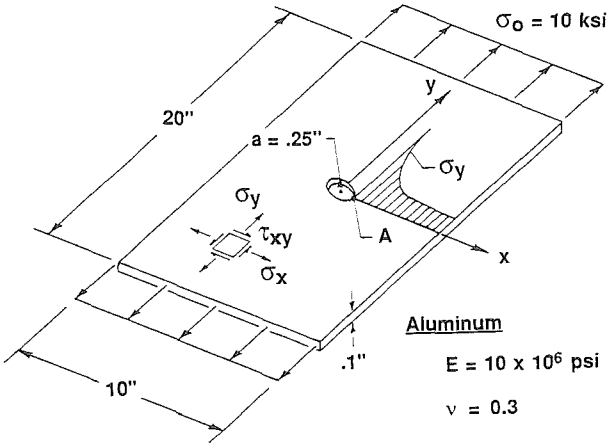


Fig. 1 Schematic of a panel with a circular cutout subjected to an applied in-plane stress.

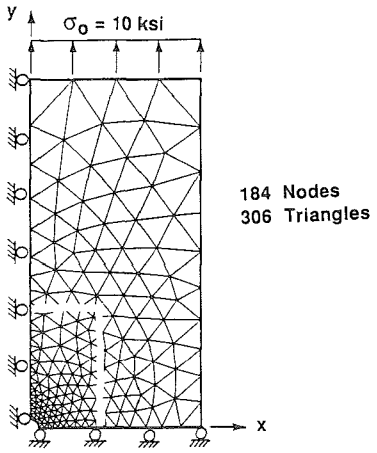


(a) Initial mesh

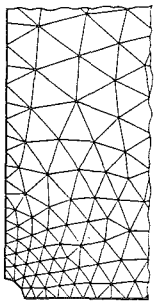

(b) Detailed mesh near the cutout

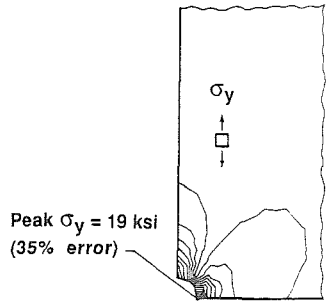


(c) Predicted stress contours

Fig. 2 Initial finite element mesh for the panel with a circular cutout and the predicted stress contours.

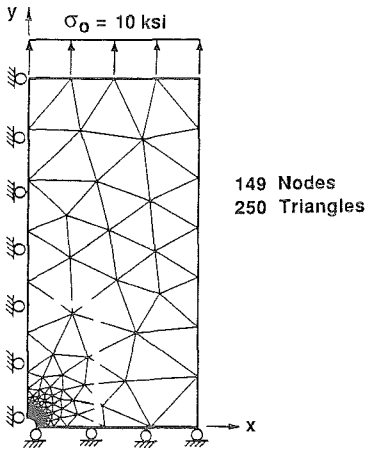


(a) Adaptive mesh

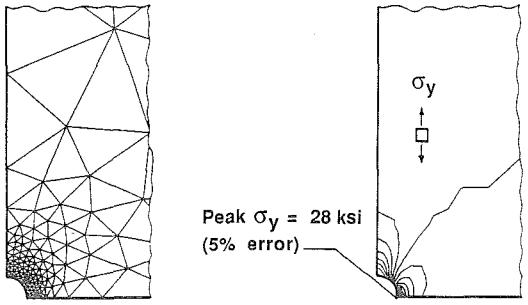


(b) Detailed mesh near the cutout

(c) Predicted stress contours

Fig. 3 Adaptive finite element mesh for the panel with a circular cutout and the predicted stress contours.

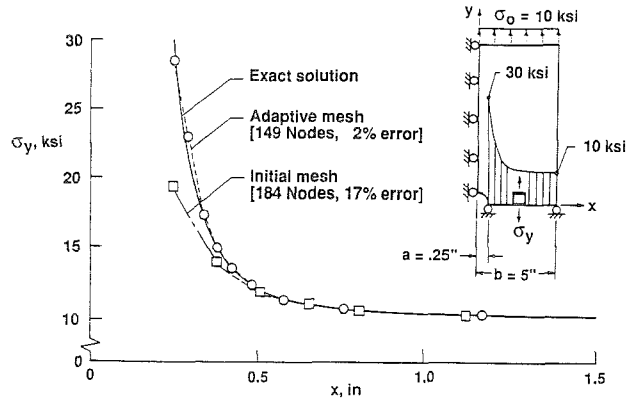


Fig. 4 Comparison of the predicted finite element and the exact stress distributions along the x-direction at y=0 for the panel with a circular cutout.

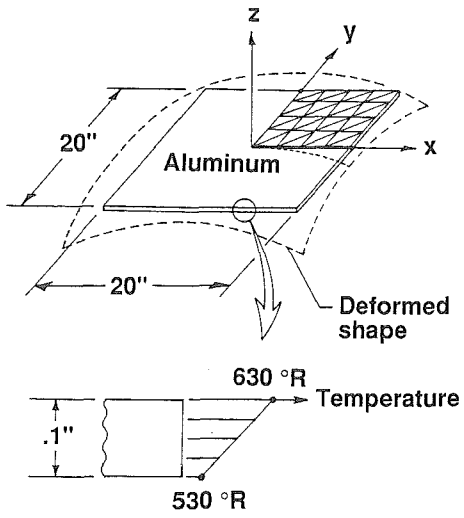


Fig. 5 Schematic of an unconstrained plate subjected to linear temperature distribution through its thickness.

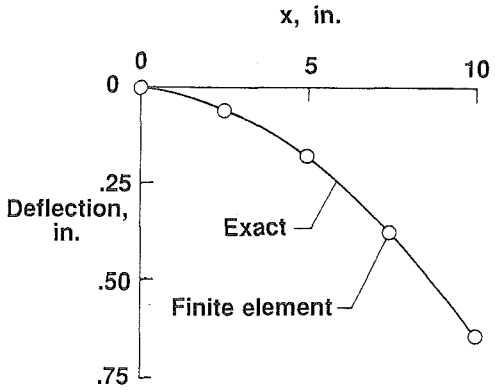


Fig. 6 Comparison of the predicted finite element and the exact transverse deflections along the x-direction at y=0 for the plate with linear temperature distribution through its thickness.

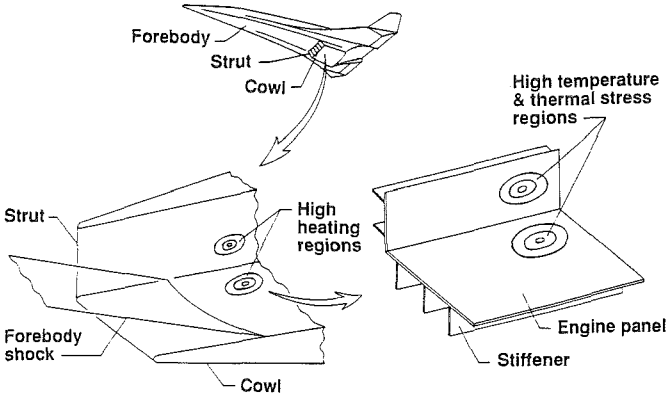


Fig. 7 Schematic of high heating and thermal stress regions on a scramjet engine inlet represented by a structure with intersecting panels.

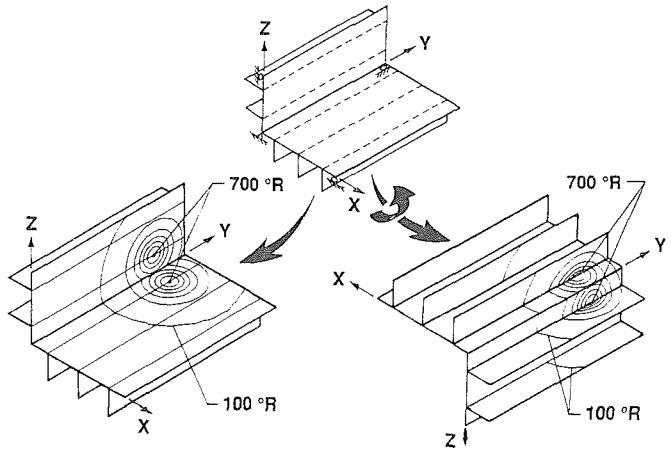


Fig. 8 Structural boundary conditions and the prescribed temperature distributions for the intersecting panels.

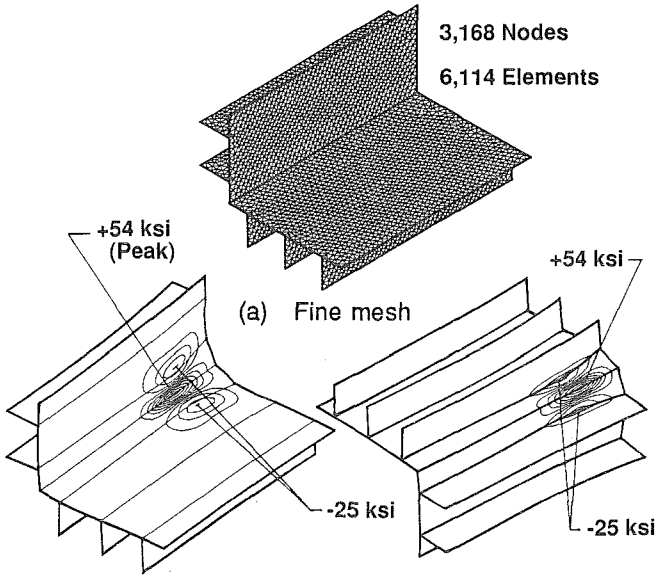


(b) Predicted axial stress contours

Fig. 9 Standard fine finite element mesh and the predicted axial stress contours on deformed configuration.

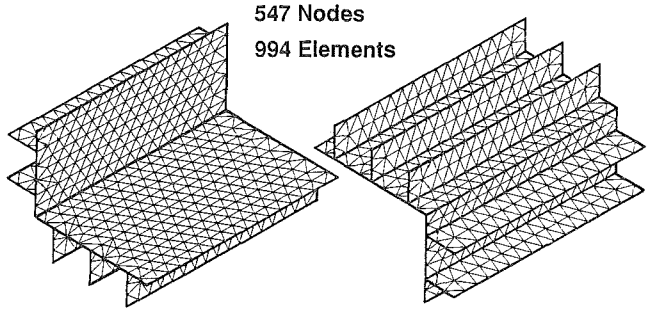


Fig. 10 Initial finite element mesh for the intersecting panels.

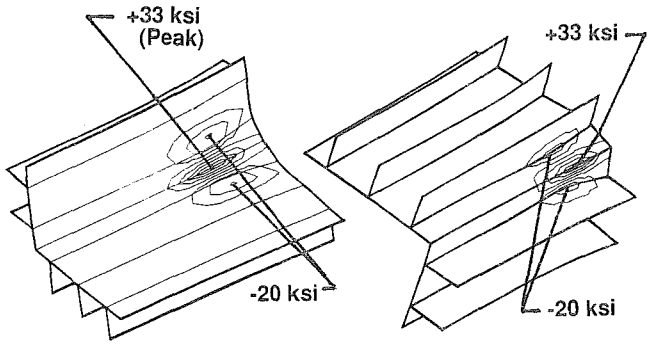


Fig. 11 Predicted axial stress contours from the initial finite element mesh on deformed intersecting panel configuration.

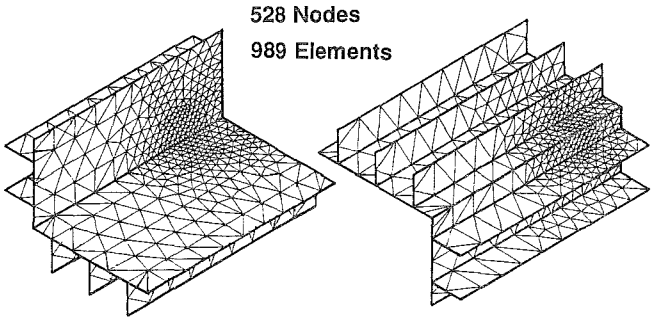


Fig. 12 Adaptive unstructured finite element mesh for the intersecting panels.

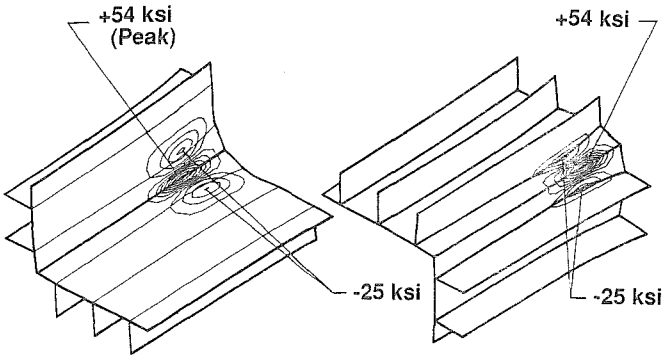


Fig. 13 Predicted axial stress contours from the adaptive finite element mesh on deformed intersecting panel configuration.